#### Research Article

Ju Qiu and Ion Stiharu\*

# Vibration and noise reduction of pipelines using shape memory alloy

https://doi.org/10.1515/secm-2022-0015 received December 07, 2021; accepted April 27, 2022

**Abstract:** In this article, the pipeline design is introduced. The new pipe structure is made of new fiber metal laminates with the unidirectional composite and sheet metal (Ti-Ni alloy). Many pipe structures are in the heating environment such as in or around the engine, which will also cause the heating-up structure. If the shape memory alloy (SMA) fiber is added to the composite lamination, it can be seen that with the increase of temperature, the stiffness of the structure is increased and so is its frequency. The changed frequency of the structure can avoid the excitation frequency in this way, which effectively inhibits the resonance. In dynamic analysis, it can also show that the pipeline with the SMA fiber has good performance for vibration reduction and noise attenuation. Additionally, the convergence of the meshing model and the effect of the thickness of the SMA material on vibration and noise reduction are also discussed.

**Keywords:** pipeline system, shape memory alloy, vibration, modes, fiber metal laminates

#### 1 Introduction

In recent years, with the rapid development of aircraft design, hydraulic piping systems have been widely used in aerospace. The pipeline is an important power part of the aircraft system, called the capillaries of the aircraft. The successful design is related to the operational safety of the entire aircraft structure and the passengers' lives, so more and more experts and researchers start to pay attention to them.

Under the internal and external excitation, the piping system generates pressure pulsations of the fluid and structural vibration of the pipeline, respectively. These vibrations can form a variety of different waves through mutual coupling. And, therefore, it forms the fluid-structure interaction of the hydraulic pipeline system. Taking an airplane pipeline system as an example, the fluidsolid coupling vibration may lead to the looseness and wear of clamps and joints, and the deformation and even fracture of the pipeline structure. The latest statistics from the US Air Force show that in the total number of aircraft system accidents, the failure of hydraulic piping systems accounts for approximately 50–60%. In the development of new aircraft in China, fatigue failure of pipelines and leakage of oil in fittings are also common. In the early 1980s, a fighter in China broke the pipeline near the engine due to the fluid-solid coupling vibration, which then caused the airplane to crash and catch fire.

With the wide use of aircraft, the failures and accidents caused by the vibration fatigue problems of pipelines have been increasing year by year, which has become one of the most difficult technical problems in aircraft systems. As aircraft hydraulic piping systems move toward high power and high pressure, some problems that had been present in the past have become more complicated. On the one hand, the fluid pulsation inside the high-pressure pipeline will cause a stronger impact, which will cause severe vibration and lead to fatigue failure, and even consequences as serious as a crash. The material of the pipeline will change under high pressure and high temperature. The thermal performance is reduced and the material of the pipeline needs to be reselected. These problems necessarily impose higher requirements on the safety design and manufacturing process of the hydraulic piping system of new aircraft.

In the past, many measures had been introduced globally for structural vibration and noise reduction.

(1) The resonance frequency of the piping structure is staggered by the surrounding excitation frequency.

<sup>\*</sup> Corresponding author: Ion Stiharu, Department of Mechanical Industrial and Aerospace Engineering, Concordia University, Montreal, QC H3G 1M8, Canada, e-mail: istih@encs.concordia.ca Ju Qiu: COMAC Shanghai Aircraft Manufacturing Co., Ltd., Composites Center, Shanghai, 200123, China; COMAC Beijing Aircraft Technology Research Institute, Beijing Key Laboratory of Civil Aircraft Structures and Composite Materials, Beijing, 102211, China; Department of Mechanical Industrial and Aerospace Engineering, Concordia University, Montreal, QC H3G 1M8, Canada

The size of the structure is partially adjusted to achieve this goal. This will increase the weight of it.

- (2) Minimize bends or use elbows with large bending radii and increase the length of bends to allow fluids to flow smoothly to reduce the vibration intensity. It cannot be used in some narrow spaces.
- (3) Adjust the number of support structures or bolsters. By changing it, the frequency can be changed to avoid resonance. This will increase the process and weight.
- (4) In the piping system, the damper or wall is coated with damping material to reduce vibration, which will also add to the process and weight.

The existing methods of noise reduction for pipeline structures and the corresponding drawbacks are listed as follows:

- Use a muffler (increasing sound-absorbing lining) to reduce noise, which will add to some processes and weight.
- (2) Reduce noise by sound-absorbing materials coated on the inner wall of the pipeline, which will add to some processes and weight.
- (3) Use a bandage for acoustic insulation (a combination of dampening materials, sound-absorbing materials, and sound insulation materials for pipeline components) to cut down noise, which also increases the weight.
- (4) Build soundproof rooms for noise reduction, which is unrealistic for moving tools such as aircraft.
- (5) Noise reduction by building soundproof screens can be realized on the highway but is not realistic for aircraft.

According to the description above, the problem of the vibration and pipeline service life in aircraft hydraulic piping systems has been handled by many scholars, but there are still many issues to be solved in design and manufacturing, such as additional weights and process, and infeasible zones.

In the current research, when the fiber of the shape memory alloy (SMA) is added to the laminated composite or metal pipe, the reduction of vibration and noise is observed with the temperature increasing. Actually, lots of scientists have been studying the mechanic properties and application of SMA.

Lester et al. [1] retrospected the extraordinary properties of SMAs. Fang et al. [2] showed the thermal–mechanical behavior, hysteretic modeling, and seismic application of superelastic NiTi SMA cables. Farber et al. [3] showed a review of various effects of composition and 3D-printing process parameters on changes in transformation characteristics, as well as possible methods for SMA' prevention and

post-process heat treatments. Liu et al. [4] presented that the new features of SMAs that resulted from first transforming the heat treatment parameter data as they were previously recorded using nonlinear mathematical relationships known to describe the thermodynamics and kinetics of phase transformations in alloys.

Baxevanis et al. [5] introduced micromechanics of precipitated near-equiatomic Ni-rich NiTi SMAs. Paranjape et al. [6] also analyzed the micromechanics' performance of polycrystalline SMAs. You et al. [7] investigated the influence of the thermomechanical coupling on the fatigue crack growth in NiTi SMA.

Li and Su [8] represented that a phase-field study of the martensitic detwinning in NiTi SMAs under tension or compression. Šesták et al. [9] introduced the response of three NiTi allotropes to compressive uniaxial loading by using the density functional theory. The results showed that the presence of relatively low compressive stresses made NiTi martensite energetically more favorable in monoclinic structures than in orthorhombic structures.

Asadi et al. [10] showed nonlinear dynamics of SMA-fiber-reinforced composite beams subjected to a primary/secondary-resonance excitation. Nekouei et al. [11] showed that free vibration analysis of laminated composite conical shells reinforced with SMA fibers. Alambeigi et al. [12] introduced free and forced vibration analysis of a sandwich beam considering porous core and SMA hybrid composite face layers on Vlasov's foundation.

Casciati et al. [13] displayed cable vibration mitigation by added SMA wires. Turner and Long [14] introduced many concepts for slat noise reduction by use of SMA in the airframe. Corbi and Corbi [15] revealed macromechanical modeling of pseudo-elasticity in SMAs for structural applications.

Huang et al. [16] introduced that the actuator was composed of a U-shaped SMA wire that was sandwiched between layers of stretched and unstretched thermal elastomer. Hadi et al. [17] demonstrated that the robot utilized a simple mechanism based on SMA actuators for adjusting the contact force between the robot and the inner wall of the pipe, to detect and repair the faults existing in pipes and narrow ducts in the industry.

Therefore, based on the superelasticity of SMA at a high temperature, it is applied to the design of the thermal structure of the aircraft pipeline. The SMA fiber is embedded in the first, middle, and last layer of the pipeline to form an SMA fiber hybrid laminated tube, to increase the stiffness of the heated pipe, thereby increasing the natural frequency of the structure. There is a good measure to control and improve the vibration and noise problems.

#### 2 The selection of pipeline materials

#### 2.1 Applications of SMA

Most SMAs use bioengineering, but it is also widely used in other fields. From the aerospace perspective, some breakthroughs have been made in the use of SMAs.

In 1969, Raychem Company in the United States produced Ti-Ni-Fe alloy fittings for the connection of hydraulic piping systems on the F14 fighter, which had avoided oil spills since then.

In 1970, American scientists made Ti-Ni wire into an antenna for spacecraft (Figure 1). It is compressed into a small iron ball at a low temperature, whose volume is only one-thousandth of the original, so it can easily be sent to the moon. As the temperature of the antenna rises, it returns to its original shape so that it can work normally to send information to the earth.

In 1997, NASA used the restoring force generated by the temperature transition of the Ni-Ti wire to achieve the opening and closing of the Mars probe solar panel.

Boeing used an SMA-indented spigot on a turbofan engine (GE-115B) (Figure 2). When the aircraft takes off and climbs, the high-temperature gas ejected causes structural deformation. The serration extends into the airflow to intervene in the mixing of the airflow, so that smooth air can reduce noise, but the thrust of the engine also slightly decreases. In the cruise phase without considering the noise-disturbing problem, the surrounding

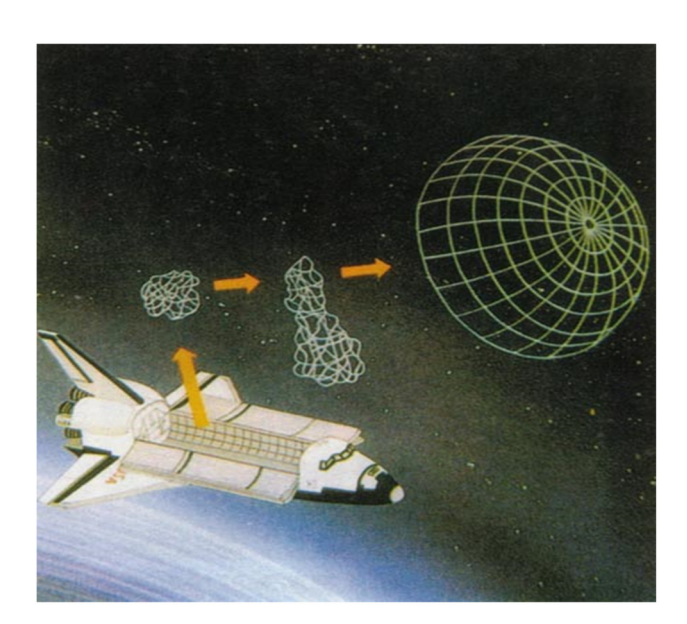


Figure 1: Spacecraft antenna.

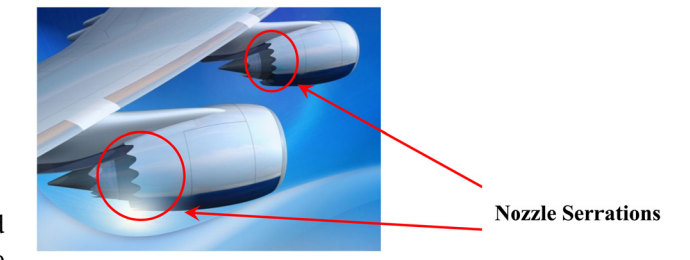


Figure 2: SMA serrated nozzles for a turbofan engine.

air is relatively cool, and the SMA reversely changes. Under this effect, the saw tooth returns to the initial state and the engine thrust is restored to the original level.

SMAs are also used in helicopters' intelligent horizontal rotors (Figure 3).

#### 2.2 New materials for piping systems

In general, aeronautical pipeline walls are made of aluminum alloy and composite materials. Due to the thermal load, the pipelines need to be thermally managed and analyzed. The requirements for explosion protection should be met. In this project, SMA materials are used in the ply design of aviation pipeline walls. The plies are shown in Figure 4.

#### 3 The thermal environment of piping vibration

The temperature and gradient changes of the pipeline are defined based on actual measurements or existing data in the aircraft environmental control system.

In hot environments, we investigate the disadvantages of the pipeline structure in the following aspects.



Figure 3: Helicopters' intelligent horizontal rotors.



Figure 4: Lamination of pipelines.

- a) The pipeline is situated in the normal temperature environment during the assembly on the ground.
   During the flight test, with the increase of the temperature, the thermal expansion of the pipeline causes a large deformation.
- As the temperature increases, the material strength performance decreases and the load-bearing capacity of the wall also declines.
- c) The internal medium of the pipeline in a certain working pressure, which is combined with the thermal load, causes the inherent dynamic characteristics to change.
- d) At high temperatures, the wall vibration is amplified.

#### 4 Causes of pipeline vibration

To study the causes of vibration in aviation pipelines, one can usually do the following:

- a) The vibration from the supporting foundation and the connection equipment.
- b) The vibration caused by the fluid pressure pulsation in the tube.
- The resonance caused by in-tube fluid vortex and air columns.

## 5 Simulation analysis of thermal vibration coupling of the pipeline

In the case of thermo-shock coupling, the thermal load on the structure not only degrades the mechanical properties of the structural material and causes uneven thermal deformation and thermal stress in the internal structure, but also changes the inherent vibration characteristics of the structure, significantly reducing the bearing capacity of the pipeline.

According to the aforementioned, the commercial large-scale software that meets the airworthiness requirements is used to model and analyze the fluid-structure coupled vibration problem of the aviation pipeline, and builds up the temperature boundary and vibration load boundary conditions. In terms of the active SMA and the non-active SMA fiber, the frequency, vibration displacement, and the sound intensity level were extracted to examine the heat-resistant properties of the heated SMA fiber tubes.

## 5.1 Characteristics of SMA material parameters

SMA materials also have phase transitions and reversibility. They have different temperatures, such as  $M_s$  and  $M_f$ , or  $A_s$  and  $A_f$ , respectively (Figure 5).

### 5.2 Mathematical model of the SMA fiber composite tube

The SMA fiber is embedded in the matrix material to form a fiber laminate. According to the equivalent theory of the composite material, considering the recovery stress of SMA and the thermal stress of the matrix, the constitutive equation of SMA fiber laminate is written as equation (1).

$$\begin{cases}
\sigma_{1} \\
\sigma_{2} \\
\tau_{12}
\end{cases} = 
\begin{bmatrix}
Q_{11} & Q_{12} & 0 \\
Q_{21} & Q_{22} & 0 \\
0 & 0 & Q_{66}
\end{bmatrix} 
\begin{cases}
\varepsilon_{1} \\
\varepsilon_{2} \\
\gamma_{12}
\end{cases}$$

$$+ 
\begin{cases}
\sigma_{r} \\
0 \\
0
\end{cases} 
\nu_{a} - 
[Q]_{m} 
\begin{cases}
\alpha_{1} \\
\alpha_{2} \\
0
\end{cases} 
\nu_{m} \Delta T, \tag{1}$$

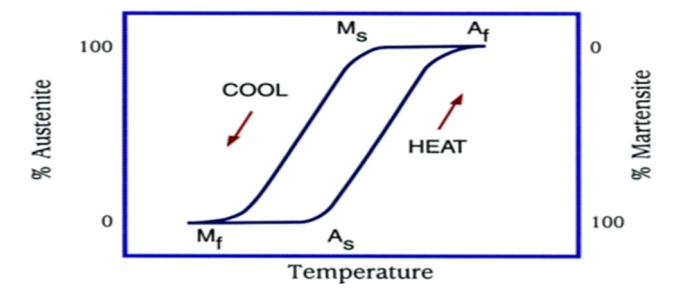


Figure 5: The process of the transformation.

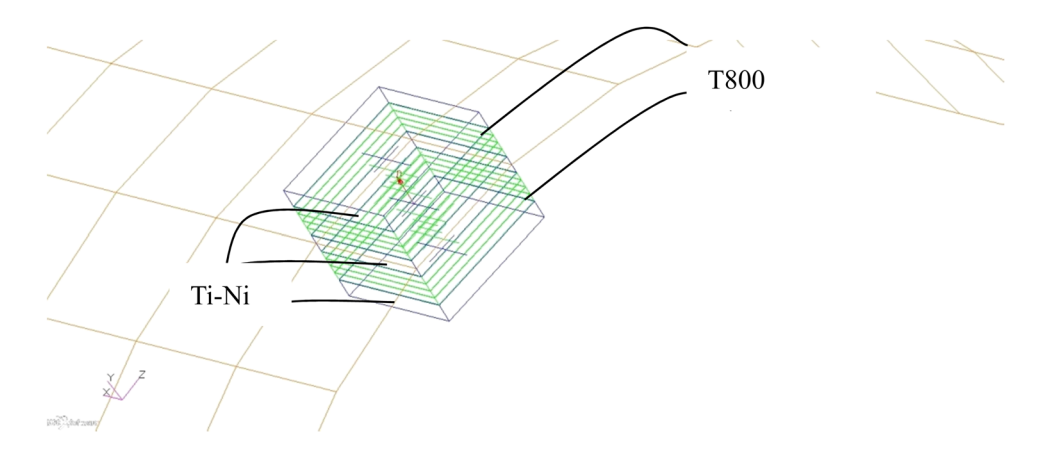


Figure 6: Lamination of the pipeline.

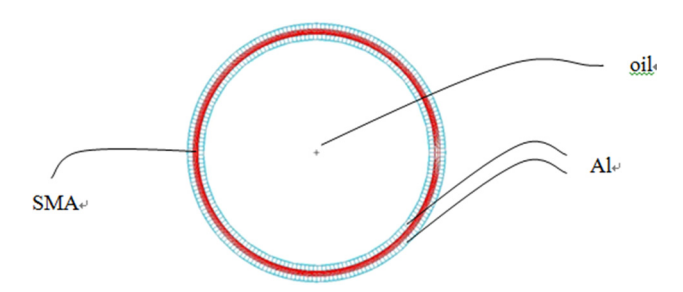


Figure 7: Lamination of metal pipe section.

where [Q] is the degraded stiffness matrix of the composite,  $v_a$  is the volume percentage of SMA in the material,  $\sigma_r$  is the recovery stress generated during the heating process of the fiber direction,  $[Q]_m$  is the retreat stiffness coefficient of the substrate,  $v_m$  is the volume percent of the matrix, and  $\alpha$  represents the thermal expansion coefficient. The relationship between the degraded stiffness matrix and engineering elastic constants is listed in equation (2).

$$Q_{11} = \frac{E_1}{1 - \mu_{12}\mu_{21}}, \quad Q_{12} = \frac{\mu_{12}E_2}{1 - \mu_{12}\mu_{21}},$$

$$Q_{22} = \frac{E_2}{1 - \mu_{12}\mu_{21}}, \quad Q_{66} = G_{12}.$$
(2)

Considering that the material parameters are related to the fiber content, it can be obtained based on the mixed rate of the multicell model in equation (3).

$$E_{1} = E_{a}v_{a} + E_{m}v_{m},$$

$$E_{2} = \frac{E_{a}E_{m}}{E_{a}v_{m} + E_{m}v_{a}},$$

$$\mu_{12} = \mu_{a}v_{a} + \mu_{m}v_{m},$$

$$G_{12} = \frac{G_{a}G_{m}}{G_{a}v_{m} + G_{m}v_{a}}.$$
(3)

Table 1: SMA material parameters

Item		Value
Elastic modulus	Austenite (A)	67 GPa
	Martensite (M)	26.7 GPa
Phase-transition temperature	$M_{\rm s}$	18.4°C
	$M_{\mathrm{f}}$	9°C
	$A_{s}$	34.5°C
	$A_{f}$	49°C
Limit recovery strain	$oldsymbol{arepsilon}_{L}$	0.067
Thermal elastic modulus	$\theta$	0.55 MPa/°C
Phase-transition constraints	$C_{M}$	8 MPa/°C
	$C_{A}$	13.8 MPa/°C
	$\sigma_{\rm s}^{\rm cr}$	100 MPa
	$\sigma_{ m f}^{ m cr}$	170 MPa
Density	ρ	$6,500 \text{ kg/m}^3$

Using the Hamilton principle and the finite element method, considering the SMA fiber laminate subjected to external forces, the control equation can be written in equation (4).

$$[M]\{\dot{U}\} + \left\{ [K_{L}] + [K_{SMA}] - [K_{VT}] + \left[ \frac{1}{2} K_{N1} \right] + \left[ \frac{1}{3} K_{N2} \right] \right\} \{U\} = \{F(t)\},$$
(4)

where [M] and  $[K_L]$  represent the mass matrix and the linear stiffness matrix of the structure;  $[K_{SMA}]$  and  $[K_{\Delta T}]$  represent the geometric stiffness matrix caused by the SMA recovery stress and the matrix thermal stress, respectively;  $[K_{N1}]$  and  $[K_{N2}]$  are stiffness matrices with displacements into first and secondary nonlinear relationships. Since stiffness matrices are related to temperature, they can be solved incrementally;  $\ddot{U}$  and U are acceleration and displacement vectors at discrete nodes of the structure.

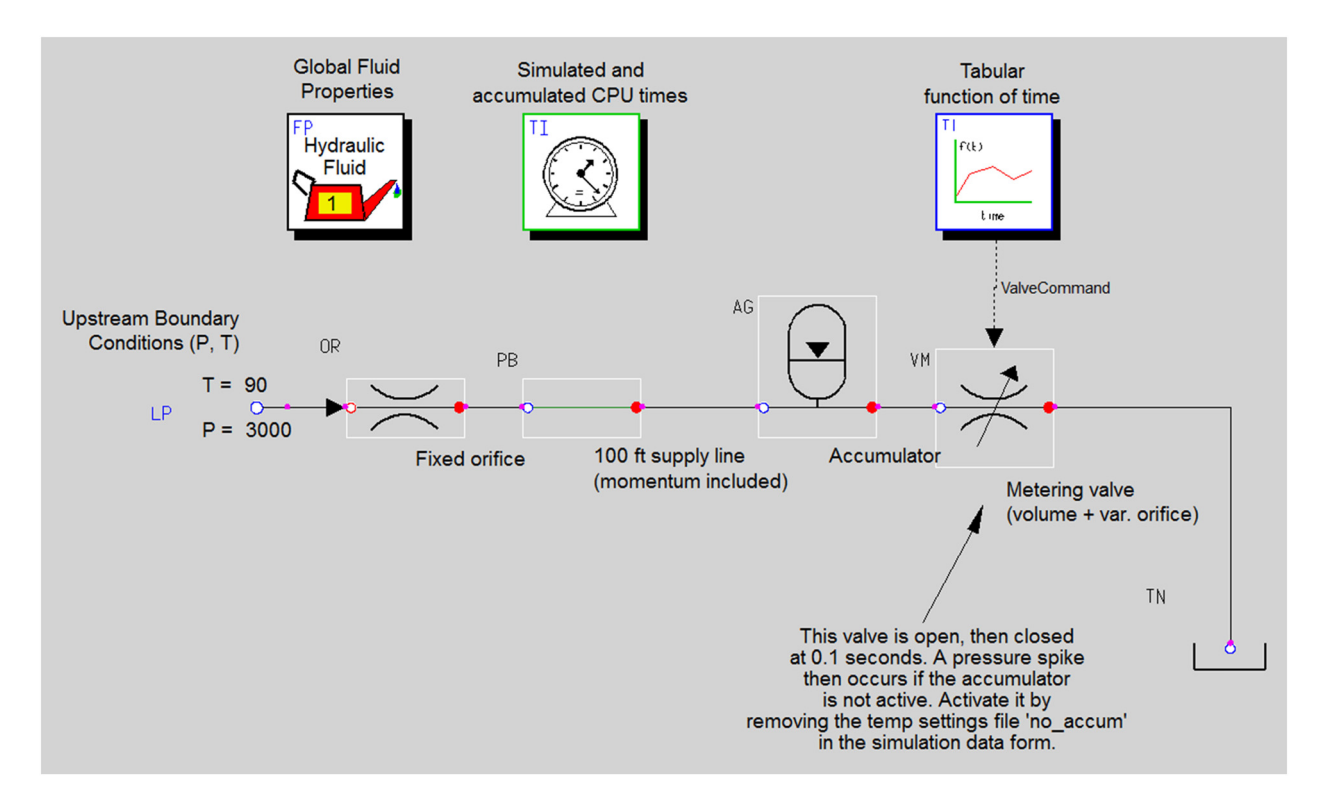


Figure 8: Waterhammer pressure simulation model.

Considering only the small deformation of the structure, which will not change the stiffness characteristics of the structure, the stiffness matrix is only related to the material properties, thermal stress and SMA recovery stress, written as  $[K] = [K_{\rm L}] + [K_{\rm SMA}] - [K_{\Delta \rm T}]$ . These parameters are all functions of temperature, which do not

change the mass matrix [M] of the structure. Therefore, during the entire analysis process, it can be considered as a structural stiffness change caused by temperature, thereby changing the modal frequency and shape. The modal parameter  $\phi$  is solved by the following formula in equation (5).

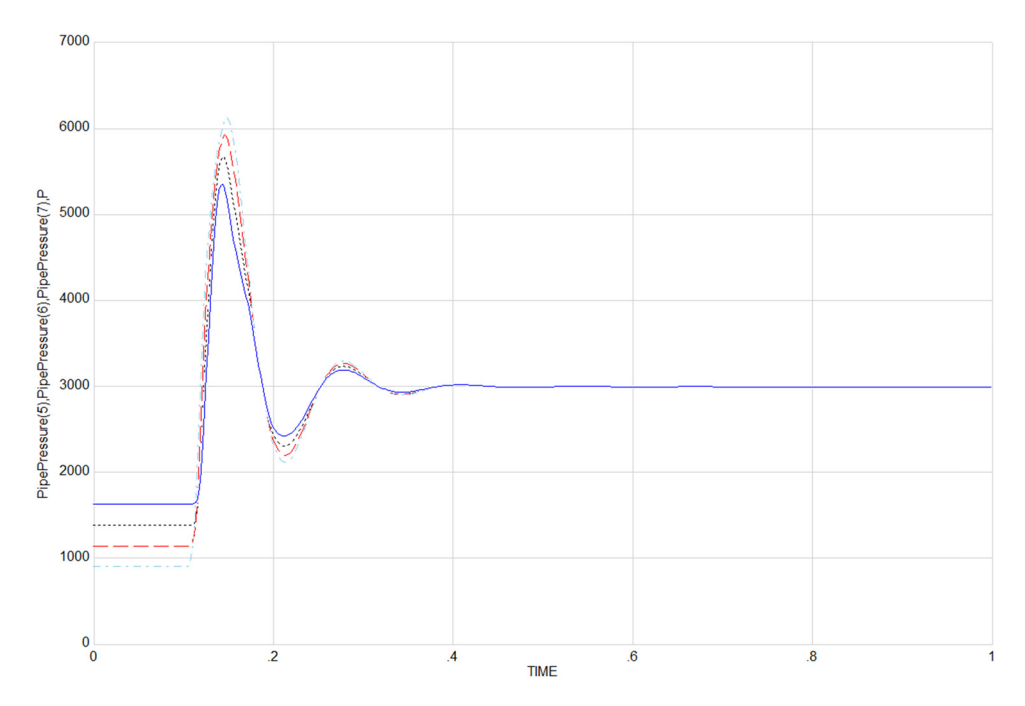


Figure 9: Pressure distributions of different sections with time.

$$([K_{\rm L}] + [K_{\rm SMA}] - [K_{\rm \nabla T}] - \omega^2[M])\{\varphi\} = 0.$$
 (5)

From the above formula, we can see that the structural stiffness characteristics change mainly in two aspects.

- a) The temperature changes the elastic modulus and temperature gradient of the material. The compressive stress generated in the structure reduces the stiffness of it.
- b) The increase of elastic modulus is caused by the phase change of SMA and the generation of recovery stress increases the stiffness of the structure.

According to the principle of fluid-structure coupling vibration of SMA pipes, the vibration equation is listed in equation (6).

$$M\ddot{U} + KU = 0, \tag{6}$$

where *M* and *K* are the structure's consistent mass matrix and the total stiffness matrix, respectively;  $\ddot{U}$  and U are the acceleration and displacement vectors of the discrete nodes of the structure, respectively.

Coupling oil or air with the tube wall forms a fluidsolid coupling matrix and the mass and stiffness of oil or air form a matrix, which is simply written in equation 7.

$$\begin{bmatrix} K_{SS}(\omega) & K_{SF} \\ B_{FS}(\omega) & A_{FF}(\omega) \end{bmatrix} \begin{Bmatrix} U_{S} \\ P \end{Bmatrix} = \begin{Bmatrix} F_{SS} \\ 0 \end{Bmatrix}, \tag{7}$$

where  $K_{SS}$  is the dynamic stiffness matrix;  $K_{SF}$  is the fluidsolid coupling matrix;  $B_{\rm FS}$  is the fluid-solid coupling coefficient.  $U_S$  and P are vectors related to structure and fluid, respectively.  $A_{\rm FF}$  contains a matrix of fluid mass and stiffness.  $F_{SS}$  is the excitation load vector applied to the structure.

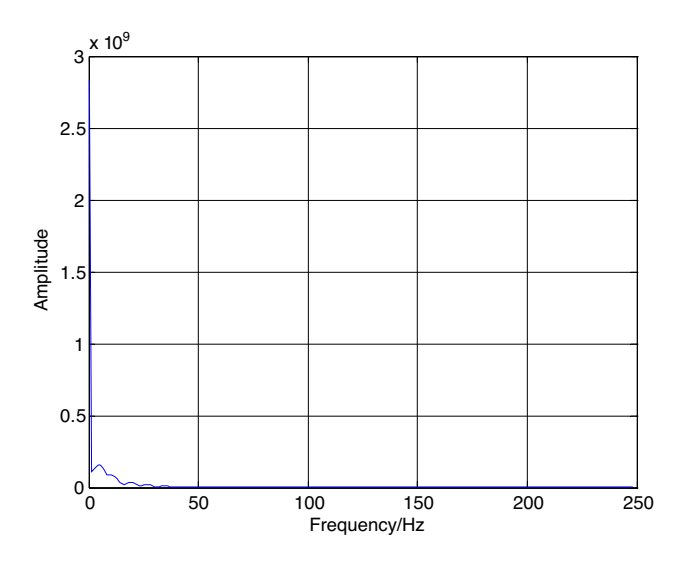


Figure 10: Frequency vs Amplitude.

#### 5.3 Models of SMA pipes

#### 5.3.1 Finite element models (FEMs)

The pipe is 1 m long, the diameter is 20 mm. The pipe wall takes two forms: one is fiber metal laminates (FMLs, Figure 6), [Ti-Ni/0/90/90/0/Ti-Ni/0/90/90/0/Ti-Ni].

The other is the mixed metal laminate pipe with the thickness of 2.5 mm (inside and outside aluminum thickness of 1 mm/Ti-Ni alloy fiber with the thickness of 0.5 mm, Figure 7).

The aluminum plate material has a Young's modulus of 70,000 MPa, a Poisson's ratio of 0.31, and a density of  $2.7 \times 10^{-9} \text{ T/mm}^3$ ; the density of the oil is  $0.8 \times 10^{-9}$ T/mm<sup>3</sup> and the sound speed is 1,324 m/s. See Table 1 for SMA material parameters.

#### 5.3.2 Boundary conditions

In general, the simulated model has two types of conditions: load boundary condition and displacement boundary condition.

#### 5.3.2.1 Load boundary condition

According to the high load caused by valve opening, the waterhammer effect of the pipeline is considered and calculated.

Waterhammer Pressure Wave Transient Analysis was done by MSC Easy 5 in Figures 8 and 9.

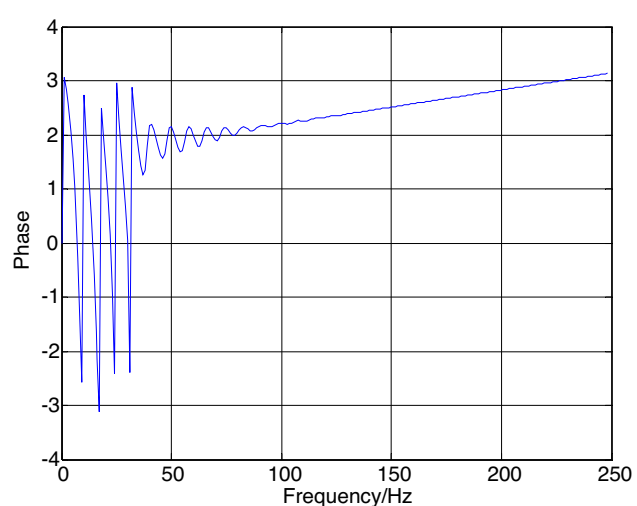


Figure 11: Frequency vs Phase.

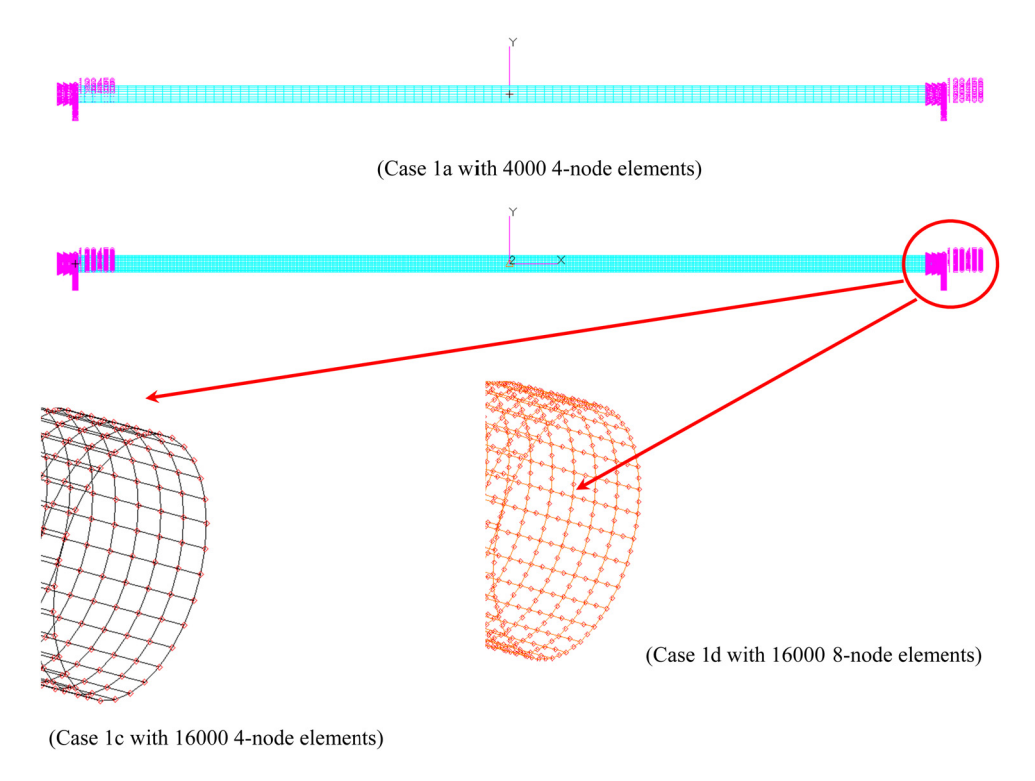


Figure 12: The FEM of the pipe. (Case 1a with 4,000 4-node elements.) (Case 1d with 16,000 8-node elements.) (Case 1c with 16,000 4-node elements.).

Usually, acoustic-induced vibration analysis is done in frequency domain. So, waterhammer transient analysis should be transferred by FFT to frequency domain. Using FFT function in MATLAB, the transform curve is shown in Figures 10 and 11.

#### 5.3.2.2 Displacement boundary condition

Two ends of the pipe were simply supported for modal analysis. In terms of the above load boundary condition, waterhammer load's phase changed little over the

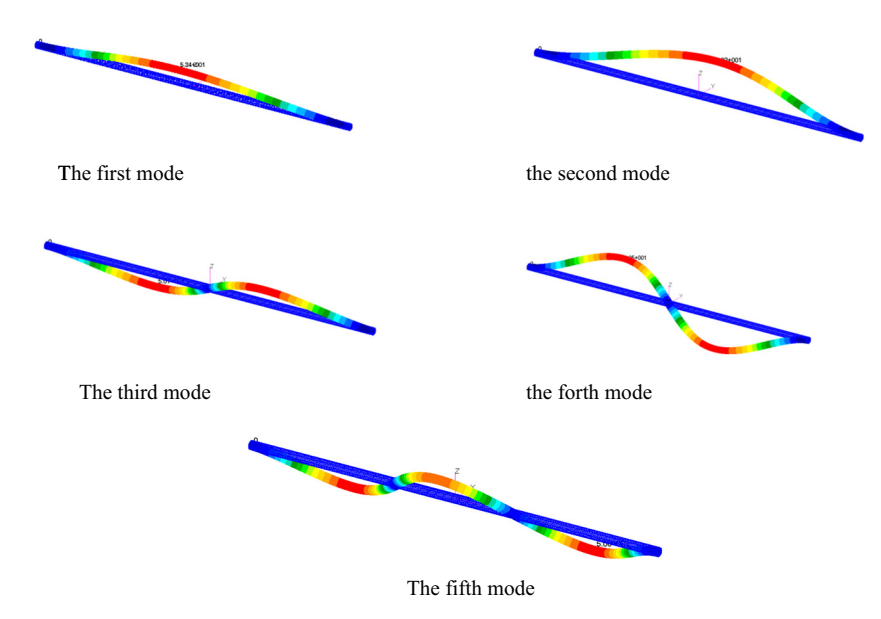


Figure 13: The first five modes' shapes.

Table 2: The first five modes for the mixed metal lamination

Conditions	Case 1a 4,000 4-node elements	Case 1b 8,000 4-node elements	Case 1c 16,000 4-node elements	Case 1d 16,000 8-node elements
First frequency (Hz)	95.24	112.90	120.28	120.76
Second frequency (Hz)	95.24	112.90	120.28	120.76
Third frequency (Hz)	265.66	302.34	328.72	329.11
Forth frequency (Hz)	265.66	302.34	328.72	329.11
Fifth frequency (Hz)	508.12	572.02	637.39	638.44

frequency and its amplitude did not change over the frequency when the frequency is more than 100 Hz. And, therefore, the unit sine force for fluid-solid coupled vibration analysis was applied to the middle of the pipe with the connector, MPC.

The wall of the pipe was defined by 2D elements and oil was set to 3D elements. The FEM of the pipe is shown in Figure 12.

It is divided into two analysis types, thermal modal analysis and thermal fluid-solid coupled vibration analysis.

In the first type of analysis, the first step is the analysis of nonlinear thermal prestress and the second one is modal analysis.

In the second of analysis, the first step is nonlinear thermal prestress analysis and the second one is fluidsolid coupled vibration analysis.

#### 5.4 Analysis of the four cases

In case 1a, 1b, 1c, and 1d, at an ambient temperature of 15° with no change, the SMA is non-active.

In case 2, at an ambient temperature of 15°, considering heating up to 100°, the SMA is active.

In case 3, at an ambient temperature of 15°, considering heating up to 200°, the SMA is active.

In case 4, at an ambient temperature of 15°, considering heating up to 250°, the SMA is active.

#### 5.5 Analyzed results

#### 5.5.1 Modal results

The first five modes' shapes are listed in Figure 13.

According to Figure 12, the mode analyses were performed for the models (Case 1a, Case 1b, Case 1c, and Case 1d) with the different size in Table 2. The modal shapes are shown in Figure 13.

Table 3: The first five modes with 16,000 4-node elements for FMLs

Conditions	Case 1c	Case 2	Case 3	Case 4	Case 2 (↑%)	Case 3 (↑%)	Case 4 (↑%)
First frequency (Hz)	100.95	110.35	120.97	125.90	9.31	19.83	24.72
Second frequency (Hz)	100.95	110.35	120.97	125.90	9.31	19.83	24.72
Third frequency (Hz)	274.07	287.21	302.78	310.25	4.79	10.48	13.20
Forth frequency (Hz)	274.07	287.21	302.78	310.25	4.79	10.48	13.20
Fifth frequency (Hz)	527.02	541.67	559.43	568.09	2.78	6.15	7.79

Table 4: The first five modes with 16,000 4-node elements for the mixed metal lamination

Conditions	Case 1c	Case 2	Case 3	Case 4	<b>Case 2</b> (↑%)	Case 3 (↑%)	Case 4 (↑%)
First frequency (Hz)	120.28	125.29	131.55	134.42	4.17	9.371292	11.75
Second frequency (Hz)	120.28	125.29	131.55	134.42	4.17	9.371292	11.75
Third frequency (Hz)	328.72	335.58	344.37	348.47	2.09	4.76	6.01
Forth frequency (Hz)	328.72	335.58	344.37	348.47	2.09	4.76	6.01
Fifth frequency (Hz)	637.39	644.91	654.65	659.23	1.18	2.71	3.43

Table 5: The max displacement and sound intensity with the different thickness of the SMA

SMA thickness	0.15 mm	0.25 mm	0.35 mm	0.5 mm
Max displacement (mm)	1.77	1.71	1.65	1.57
Max sound intensity (dB)	82	77	69	60

From the above table, the frequencies increase with the increasing number of elements. When the number reaches 16,000, the frequencies of Case 1b and Case 1c are very close. When the number reaches 16,000 with whether the linear element or nonlinear one, the frequencies of Case 1c and Case 1d are almost identical. This means the model dimension of Case 1c has a good solution precision.

Compared with active and non-active SMA, the mode results are listed in Tables 3 and 4.

#### 5.5.2 Thermal fluid-solid results

During the thermal fluid-solid coupled vibration analysis, the thicknesses of the SMA include 0.15, 0.25, 0.35, and 0.5 mm for Case 4. The peak displacement and sound intensity are shown in Table 5.

In Table 5, the max displacement and sound intensity reduce with the increasing SMA thickness, which means that adding more SMA to the structure is more beneficial to the vibration and noise reduction.

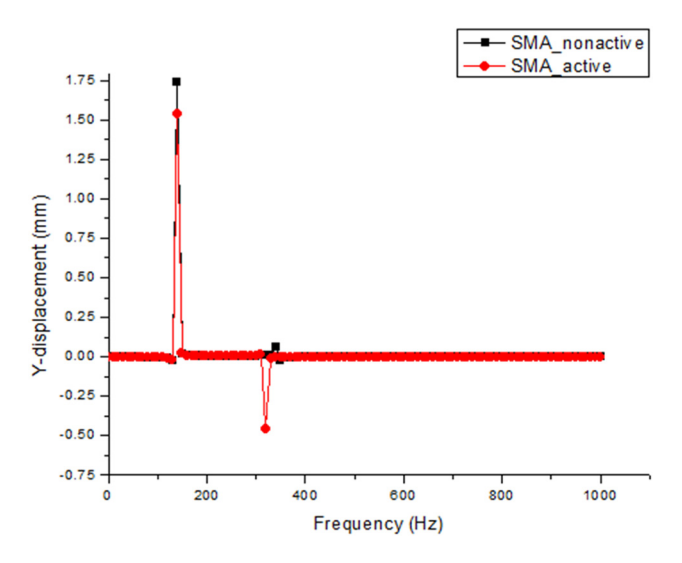


Figure 14: Comparison of vibration of the pipe under non-active and active SMAs.

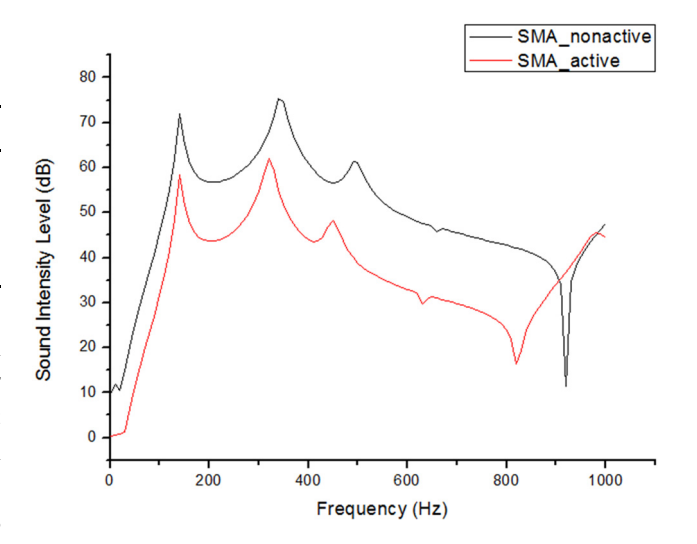


Figure 15: Comparison of sound intensity levels of the pipe under non-active and active SMAs.

After the thermal fluid–solid coupled vibration analysis, the typical results for Case 4 are listed in Figures 14 and 15.

According to the calculated results, the Y displacement results of typical nodes from the mixed metal lamination are compared (Figure 14).

As can be seen from the above picture, the highest point is around 100 Hz. If the SMA fiber is active, the vibration peak can be reduced by 11%.

When we compare the results of sound intensity levels of typical parts, we can see Figure 15.

As can be seen from the above figure, the peaks of sound intensity at around 100, 300, and 500 Hz of the typical parts can drop by about 10–20 dB under the active SMA state.

#### 6 Conclusion

At present, the existing FMLs, GLARE, is usually made of glass fiber-reinforced aluminum alloy laminates, while the proposed material in this article is made of glass fiber-reinforced Ti–Ni alloy laminate.

To the best of our knowledge, GLAREs have good impact and fatigue properties. However, with the increasing speed of the flight, the aerodynamic heating will transfer the heat to the internal structure to warm it up. There are many pipe structures in the heating environment such as in and around the engine, which will also cause the structure to heat up. If the SMA fiber is added to the aluminum tube or composite lamination, it can be seen that when the temperatures increase, the stiffness and frequency of the

structure will increase. The changed frequency of the structure can avoid the excitation frequency in this way, which effectively inhibits the resonance. In dynamic analysis, it can also be seen that the pipe with SMA fiber composites has performed well for vibration reduction and noise attenuation. According to the different thicknesses of SMA, the more SMA, the better effect of vibration and noise reduction.

#### 7 Final remarks

In this article, a new composite is described, FMLs with Ti-Ni alloy. From the history of aeronautical materials, the wing skin of the first airplane was made of a composite fabric. When the metal was processed, the performance was stable. After being used, we gradually realized that the carbon fiber or glass fiber composites had excellent properties. However, with the further development of the metal materials, will the performance of metallic materials once again exceed that of composite materials? Or, will metal and composite interwoven materials develop a lot? Or, whether the metal and composites can learn from each other's strong points and close the gap? Designers have an example of a GLARE in the last century and the other example of 3D printer for metals in this century. The proposed materials may be bound to develop worldwide.

**Conflict of interest:** Authors state no conflict of interest.

#### References

- Lester BT, Baxevanis T, Chemisky Y, Lagoudas DC. Review and perspectives: shape memory alloy composite systems. Acta Mech. 2015;226(12):3907-60.
- Fang C, Zheng Y, Chen J, Yam MC, Wang W. Superelastic NiTi SMA cables: Thermal-mechanical behavior, hysteretic modelling and seismic application. Eng Struct. 2019;183(MAR.15):533-49.
- Farber E, Zhu JN, Popovich A, Popovich V. A review of NiTi shape memory alloy as a smart material produced by

- additive manufacturing. Mater Today: Proc. 2020;30(3):761-7.
- [4] Liu S, Kappes BB, Amin-ahmadi B, Benafan O, Zhang X, Stebner AP. Physics-informed machine learning for composition - process - property design: Shape memory alloy demonstration. Appl Mater Today. 2021;22:100898.
- Baxevanis T, Cox A, Lagoudas DC. Micromechanics of precipitated near-equiatomic Ni-rich NiTi shape memory alloys. Acta Mech. 2014;225:1167-85.
- [6] Paranjape HM, Paul PP, Sharma H, Kenesei P, Park JS, Duerig TW, et al. Influences of granular constraints and surface effects on the heterogeneity of elastic, superelastic, and plastic responses of polycrystalline shape memory alloys. I Mech Phys Solids, 2017:102:46-66.
- You Y, Zhang Y, Moumni Z, Anlas G, Zhang W. Effect of the thermomechanical coupling on fatigue crack propagation in NiTi shape memory alloys. Mater Sci Eng A. 2017;685:50-6.
- Li X, Su Y. A phase-field study of the martensitic detwinning in NiTi shape memory alloys under tension or compression. Acta Mech. 2020;231:1539-57.
- Šesták P, Cerný M, Pokluda J. Energetics of NiTi allotropes [9] under uniaxial compression. Scr Mater. 2017;133:92-5.
- [10] Asadi H, Bodaghi M, Shakeri M, Aghdam MM. Nonlinear dynamics of SMA-fiber-reinforced composite beams subjected to a primary/secondary-resonance excitation. Acta Mech. 2015:226(2):437-55.
- Nekouei M, Raghebi M, Mohammadi M. Free vibration [11] analysis of laminated composite conical shells reinforced with shape memory alloy fibers. Acta Mech. 2019;230:4235-55.
- Alambeigi K, Mohammadimehr M, Bamdad M, Rabczuk T. Free and forced vibration analysis of a sandwich beam considering porous core and SMA hybrid composite face layers on Vlasov's foundation. Acta Mech. 2020;231:3199-218.
- [13] Casciati F, Faravelli L, Fuggini C. Cable vibration mitigation by added SMA wires. Acta Mech. 2008;195:141-55.
- [14] Turner TL, Long DL. Development of a SMA-based, slat-gap filler for airframe noise reduction. AIAA SciTech, 23rd AIAA/ AHS Adaptive Structures Conference; 5-9 January 2015. Kissimmee: Florida AIAA 2015-0730. p. 1-10.
- [15] Corbi I, Corbi O. Macro-mechanical modelling of pseudoelasticity in shape memory alloys for structural applications. Acta Mech. 2016;227:2171-9.
- [16] Huang X, Kumar K, Jawed MK, Mohammadi Nasab A, Ye Z, Shan W, et al. Highly dynamic shape memory alloy actuator for fast moving soft robots. Eng Struct. 2019;183:533-49.
- [17] Hadi A, Hassani A, Alipour K, Askari Moghadam R, Pourakbarian Niaz P. Developing an adaptable pipe inspection robot using shape memory alloy actuators. J Intell Mater Syst Struct. 2020;31(4):632-47.